AFRL-RW-EG-TR-2009-7066

Eigendeformation-Based Homogenization of Concrete

Wei Wu, Zheng Yuan, Jacob Fish

Multiscale Science and Engineering Center
Rensselaer Polytechnic Institute
110 8th Street
Troy, NY 12180

CONTRACT NO. FA8651-05-1-0007

March 26, 2009

FINAL REPORT FOR PERIOD May 2005 - March 2009

AIR FORCE RESEARCH LABORATORY, MUNITIONS DIRECTORATE

■ **Air Force Materiel Command** ■ **United States Air Force** ■ **Eglin Air Force Base**

NOTICE AND SIGNATURE PAGE

This report was cleared for public release by the 96 Air Base Wing, Public Affairs Office, and is available to the general public, including foreign nationals. Copies may be obtained from the Defense Technical Information Center (DTIC) <http://www.dtic.mil/dtic/index.html>.
.

AFRL-RW-EG-TR-2009-7066 HAS BEEN REVIEWED AND IS APPROVED FOR PUBLICATION IN ACCORDANCE WITH ASSIGNED DISTRIBUTION STATEMENT.

FOR THE DIRECTOR:

//Original Signed//	//Original Signed//
Azar S. Ali	Brian W. Plunkett
Technical Director	Mechanical Engineer
Assessment and Demonstrations Division	Computational Mechanics Branch

REPORT DOCUMENTATION PAGE

Form Approved
OMB No. 0704-0188

1. REPORT DATE *(DD-MM-YYYY)*	**2. REPORT TYPE**	**3. DATES COVERED** *(From - To)*
26-03-2009	FINAL	May 2005 – March 2009

4. TITLE AND SUBTITLE

Eigendeformation-Based Homogenization of Concrete

5a. CONTRACT NUMBER

5b. GRANT NUMBER
FA 8651-05-1-0007

5c. PROGRAM ELEMENT NUMBER
62602F

6. AUTHOR(S)
Wei Wu, Zheng Yuan, Jacob Fish

5d. PROJECT NUMBER
2502

5e. TASK NUMBER
24

5f. WORK UNIT NUMBER
17

7. PERFORMING ORGANIZATION NAME(S) AND ADDRESS(ES)

Multiscale Science and Engineering Center
Rensselaer Polytechnic Institute
110 8th Street
Troy, NY 12180

8. PERFORMING ORGANIZATION REPORT NUMBER

9. SPONSORING / MONITORING AGENCY NAME(S) AND ADDRESS(ES)
Air Force Research
AFRL/RWAC
101 West Eglin Boulevard
Eglin AFB, FL 32542-6810

10. SPONSOR/MONITOR'S ACRONYM(S)
AFRL-RW-EG

11. SPONSOR/MONITOR'S REPORT NUMBER(S)
AFRL-RW-EG-TR-2009-7066

12. DISTRIBUTION / AVAILABILITY STATEMENT

DISTRIBUTION A: Approved for public release; distribution unlimited. 96th ABW/PA Approval and Clearance # 96ABW-2009-0275, dated 15 Jun 2009

13. SUPPLEMENTARY NOTES

14. ABSTRACT

A two-scale approach based on eigendeformation-based homogenization is explored to predict the behavior of concrete targets subjected to impact loading by high speed projectiles. The method allows accounting for micromechanical features of concrete at a computational cost comparable to single scale phenomenological models of concrete. The inelastic behavior of concrete is modeled using three types of eigenstrains. The eigenstrains in the mortar phase include pore compaction (or lock-in), rate-dependent damage and plasticity eigenstrains, whereas the inelastic behavior of aggregates is assumed to be governed by plasticity only. Material parameters were identified using inverse methods against unconfined compression and uniaxial compression tests. A unit cell was constructed from a 3D digital image of concrete. The eigendeformation-based homogenization approach was validated for the projectile penetration into concrete target. The simulation results were found to be in reasonable agreement with the experimental data. Attention is restricted to non-reinforced concrete.

15. SUBJECT TERMS
Multi-Scale, Homogenization, Eigendeformation, Penetration, Concrete

16. SECURITY CLASSIFICATION OF:			**17. LIMITATION OF ABSTRACT**	**18. NUMBER OF PAGES**	**19a. NAME OF RESPONSIBLE PERSON**
a. REPORT	**b. ABSTRACT**	**c. THIS PAGE**			Brian W. Plunkett
UNCLASSIFIED	UNCLASSIFIED	UNCLASSIFIED	UL	31	**19b. TELEPHONE NUMBER** *(include area code)*

This material is based on research sponsored by the Air Force Research Laboratory Munitions Directorate, under agreement number **FA 8651-05-1-0007**. The U.S. Government is authorized to reproduce and distribute reprints for Governmental purposes notwithstanding any copyright notation thereon.

The views and conclusions contained herein are those of the author and should not be interpreted as necessarily representing the official policies or endorsements, either expressed or implied, of the Air Force Research Laboratory or the U.S. Government.

Table of Contents

List of Figures

Abstract

A two-scale approach based on eigendeformation-based homogenization is explored to predict the behavior of concrete targets subjected to impact loading by high speed projectiles. The method allows accounting for micromechanical features of concrete at a computational cost comparable to single scale phenomenological models of concrete. The inelastic behavior of concrete is modeled using three types of eigenstrains. The eigenstrains in the mortar phase include pore compaction (or lock-in), rate-dependent damage and plasticity eigenstrains, whereas the inelastic behavior of aggregates is assumed to be governed by plasticity only. Material parameters were identified using inverse methods against unconfined compression and uniaxial compression tests. A unit cell was constructed from a 3D digital image of concrete. The eigendeformation-based homogenization approach was validated for the projectile penetration into concrete target. The simulation results were found to be in reasonable agreement with the experimental data. Attention is restricted to non-reinforced concrete.

1. Introduction

Portland concrete has been widely used as a construction material for civil and military applications since the 18th century, even though its grandfather, Roman concrete made from quicklime, pozzolanic and an aggregate of pumice, dates back to Roman Empire. The reasons for concrete's ubiquity in practice are not only it being one of the environmentally friendliest and cost-effective materials, but also due to its high compressive strength, which makes it play a critical role in defense applications including nuclear reactor containments and fortification installations.

The problem of predicting the behavior of concrete targets subjected to impact loading by high speed projectiles has been of military interest for many years. Various procedures have been developed and they generally fall into three categories: (1) empirical or analytical approaches [1,2], (2) experimental approaches [3-5] and (3) numerical approaches [6-15].

For numerical approaches, such as the finite element method, to be viable, it is essential to characterize the constitutive models for concrete. Concrete is typically modeled as a homogeneous single-scale [7-11,16,17] or heterogeneous two-phase [6,12-14] material. In an attempt to capture the dilatant behavior of concrete the cap plasticity model was employed in [7,8]. In [9], a modified Holmquist-Johnson-Cook (HJC) model for concrete with enhanced pressure-shear behavior, strain-rate sensitivity and additional damage variables tracking the tensile/shear cracking and pore compaction were introduced. A coupled plasticity-damage model was considered in [10], whereas an energy release rate based plasticity-damage model was suggested in [11]. In [17] a microplane model of concrete was developed to account for pressure sensitivity, dilatancy, deviation from normality, Bauschinger effect and hysteresis.

Consideration of concrete as a heterogeneous or composite material consisting of mortar and aggregates has been somewhat less popular (see [6,12-14] for noteworthy exceptions), The premise of this approach is that each phase can be modeled using different material laws and the interaction between the phases can be explicitly accounted for. This is of particular importance

since elastic degradation of mortar exhibits a more compounded process than that of the aggregate. In the mortar phase, microcrack closure under reversal loading gives rise to stiffening of material and microcrack growth is not perfectly brittle but rather involves plastic deformations. On the other hand, the aggregate phase can be adequately described within the framework of classical plasticity. The interaction between the phases so far have been predominantly accounted for by means of various effective medium models, such as Mori-Tanaka and self-consistent approaches. Notable exceptions were reported in [18-20] where computational homogenization methods were employed to explicitly account for concrete microstructure. Also noteworthy are various mesomechanical models where continuum is replaced by discrete medium [21, 22].

While computational cost of the computational homogenization approaches is a small fraction compared to the direct numerical simulation, where a characteristic mesh size is of the heterogeneity order, they remain computationally prohibitive for complex microstructures such as those of concrete. This is because a nonlinear unit cell problem for a two-scale problem has to be solved for a number of times equal to the product of the number of quadrature points at a macroscale and the number of load increments and iterations at the macroscale. If this approach is to be a viable alternative to modeling concrete, it is necessary to reduce the computational complexity of the fine scale (unit cell) problem without significantly compromising on the solution accuracy of interest, which is typically at the macro level. In this manuscript we explore the application of the eigendeformation based homogenization [23-28] to multiscale modeling of the non-reinforced concrete targets subjected to impact loading by high speed projectiles. The salient feature of the eigendeformation-based homogenization is that the unit cell problem is formulated in terms of eigendeformation modes, which *a priori* satisfy equilibrium equations in the microscale, and thus eliminate the need for costly solution of discretized nonlinear equilibrium.

The paper is organized as follows. The problem statement is formulated in Section 2. The formulation of eigenstrains and the overall solution algorithm are given in Section 3. Validation studies are considered in Section 4 starting with the digital image of the concrete microstructure, calibration of microphase properties and prediction in a penetration problem. Finally, several concluding remarks are drawn in Section 5. The eigendeformation-based homogenization theory is outlined in the Appendix.

2. Problem Statement

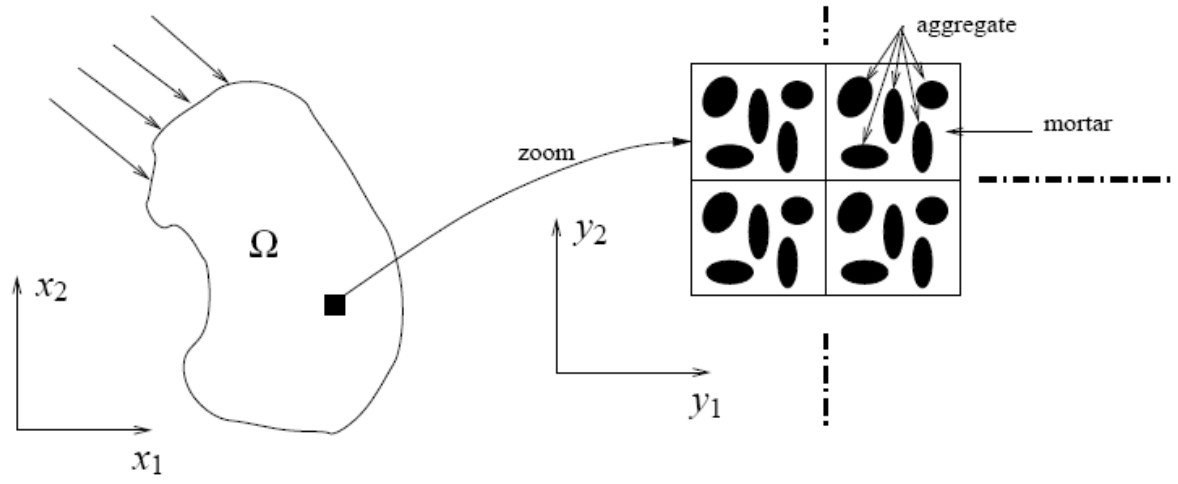

Figure 1. Macro- and micro- structure of concrete material

Consider a concrete as a heterogeneous material formed by a repetition of locally periodic microstructure as shown in Figure 1. The microstructure consisting of *mortar* and *aggregate* phases is described by a unit cell or so-called representative volume element (RVE).

The macroscopic problem considered in the paper is a penetration example [4] by a rigid projectile as shown in Figure 2. The projectile geometry is given in Figure 3. The physical properties of the concrete used in this paper are listed as Table 1.

The governing equations describing the response of the structural system are:

Momentum balance:

$$\sigma_{ij,j}(x,t) + b_i(x,t) = \rho(x,t)\ddot{u}_i(x,t), \tag{1}$$

where σ_{ij} is stress, b_i is body force, ρ is density and u_i is displacement.

Kinematics relation:

$$\dot{\varepsilon}_{ij}(x,t) = \frac{1}{2}\left(\frac{\partial \dot{u}_i}{\partial x_j} + \frac{\partial \dot{u}_j}{\partial x_i}\right), \tag{2}$$

where u_i, ε_{ij} are displacement and strain components, respectively. The superimposed dot denotes material time derivative.

Constitutive relation:

$$\sigma_{ij}(x,t) = L_{ijkl}(x)\left[\varepsilon_{kl}(x,t) - \sum_I {}^I\mu_{kl}(x,t)\right] \tag{3}$$

where L_{ijkl} is elastic moduli and ${}^I\mu_{ij}$ is the *I*-th component of the eigenstrain We assume an additive decomposition of total strains into elastic strains and eigenstrains consisting of inelastic strains (damage, plasticity, etc.), hygrothemal strains, and phase transformation strains. The

formulation of the inelastic deformation strains is detailed in Section 3.

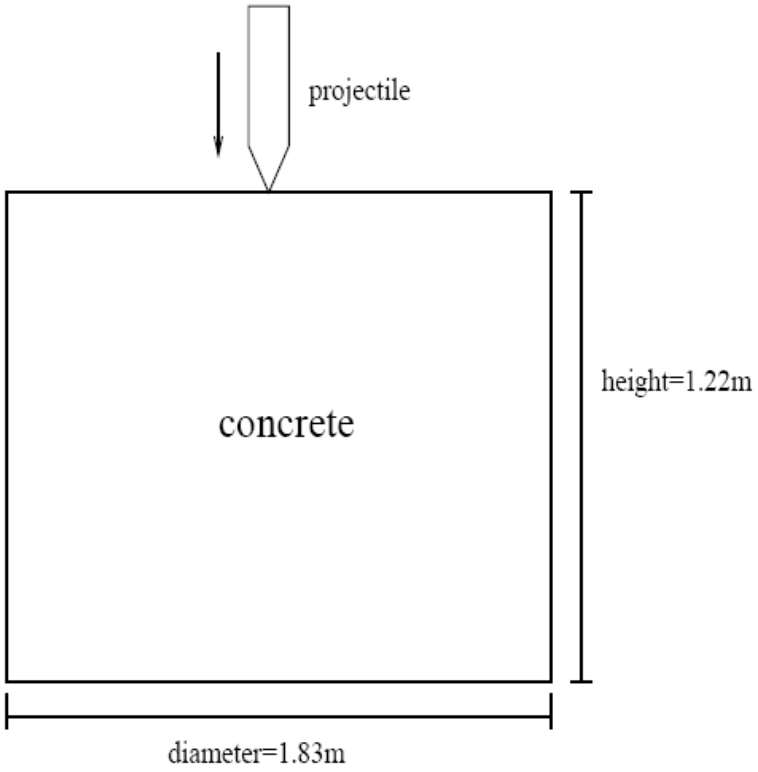

Figure 2. Definition of the penetration model

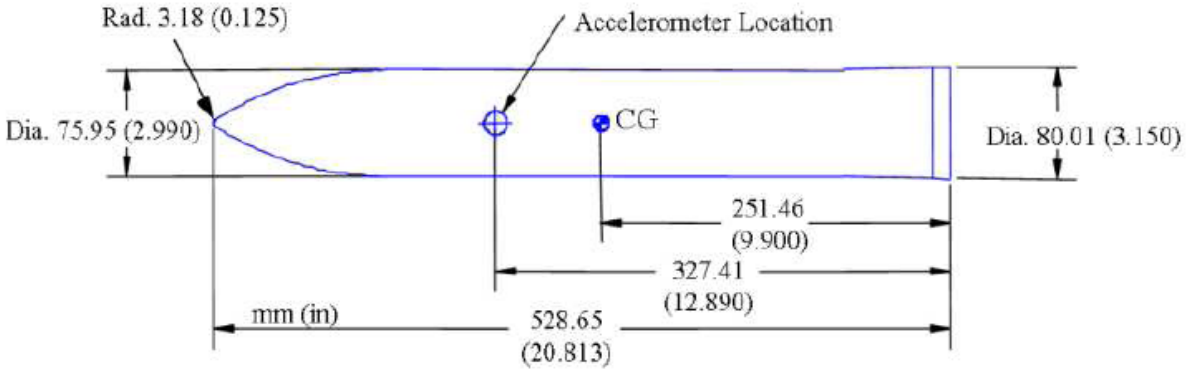

Figure 3. The geometry of 3.0 CRH projectile [4]

Table 1. Physical properties of concrete used in the paper

Compressive strength	38.7MPa
Wet density	2.25 Mg/m^3
Volume solids	82.53%
Volume water	5.63%
Volume air	11.84%
Volume voids	17.47%

The mixture portions of the concrete (38.7MPa) are listed as Table 2.

Table 2. Mixture portions of concrete used in the paper

Materials	Mass in pounds
ASTM Type I, Holnam Cement Co.	543
Natural, siliceous, concrete sand, SSD condition	1478
ASTM No.89, 3/8 NMS, crushed limestone, SSD condition	1566
Water reducer, high-range, Eucon 37	961 ml or 32.5 fl oz
Water reducer, normal-range, Eucon WR-91	961 ml or 32.5 fl oz
Water	315

3. Microscale Inelastic Properties of Concrete: Eigenstrain

The theoretical framework of the eigendeformation-based approach is outlined in Appendix A. In this Section we focus on the formulation of the inelastic deformation eigenstrains ${}^{I}\overline{\mu}_{ij}$ assuming perfect interfaces, i.e., neglecting the eigenseparations $\overline{\delta}_{\hat{n}}$. Having been frequently referred to as plastic-fracturing materials, concrete exhibits plastic flow in both mortar and aggregate phases. We hereby define plastic strain ε^{p} as one source of the eigenstrains in both phases. Another source of eigenstrains denoted as ε^{d} is formed by crack nucleation and microcracks growth, which typically takes place in the mortar phase [13]. Finally, the closure of microcracks and/or original air voids under compressive load gives rise to the compaction of concrete material. This causes a sudden stiffening of the mortar phase [9,13] known as lock-in. This phenomenon in the mortar phase will be modeled by so-called lock-in eigenstrain denoted as ε^{c}. The next two subsections will focus on the formulation of the eigenstrains in the two phases. The algorithm details will be given in Section 3.3.

3.1. Eigenstrains in the aggregate phase

The inelastic behavior of aggregates is modeled using classical isotropic/kinematic plasticity theory. Thus plastic strain is assumed to be the only eigenstrain source

$$\overline{\mu}^{(agg.)} = \varepsilon^{p(agg.)}. \tag{4}$$

The inelastic parameters for the aggregate phase are: hardening modulus $\overline{H}^{(agg.)}$, yield stress as $\sigma_{Y}^{(agg.)}$, and mixture parameter $\theta^{(agg.)}$ defining the relative weight of the isotropic and kinematic hardening ($\theta^{(agg.)}=1$ for pure isotropic hardening and $\theta^{(agg.)}=0$ for pure kinematic hardening). Two additional internal variables denoted $[a,b]$ are defined with a being the equivalent plastic strain, and b tracking the center of von Mises yield surface in the stress deviator space. Given local strain in the aggregate $\varepsilon_{ij}^{(agg.)}$, one can find local plastic strain $\varepsilon_{ij}^{p(agg.)}$ by radial return or similar algorithm [29].

3.2. Eigenstrains in the mortar phase

We assume that the three sources of eigenstrains $\varepsilon^{p(mortar)}$, $\varepsilon^{d(mortar)}$, $\varepsilon^{c(mortar)}$ introduced in Section 3 may not evolve simultaneously. The damage eigenstrain $\varepsilon^{d(mortar)}$ is assumed to be initiated and accumulated under tensile loading at the microscale, while $\varepsilon^{p(mortar)}$ and $\varepsilon^{c(mortar)}$ evolve under compressive loading. The tensile and compression loadings are determined by probing the macroscopic volumetric strain $\Xi=\sum_{I=1}^{3}\overline{\varepsilon}_{I}$, where $\overline{\varepsilon}_{I}$ is a macroscopic principal strain. The evolution of the inelastic deformation eigenstrain for mortar is then expressed as

$$\begin{cases} \dot{\bar{\mu}}^{(mortar)} = \dot{\varepsilon}^{p(mortar)} + \dot{\varepsilon}^{c(mortar)} & if\ \Xi \le 0, \\ \dot{\bar{\mu}}^{(mortar)} = \dot{\varepsilon}^{d(mortar)} & if\ \Xi > 0. \end{cases} \tag{5}$$

For plastic strain $\varepsilon^{p(mortar)}$, we employ the same linear isotropic/kinematic hardening law as for the aggregate phase. The formulation of the other two eigenstrain components in the mortar phase is discussed next.

3.2.1. The damage eigenstrain $\varepsilon^{d(mortar)}$

We consider a rate-dependent damage model to alleviate (at least partially) mesh size dependency caused by strain softening. For simplicity, we omit the superscript (mortar). The damage parameter ω is defined to be a function of equivalent strain $\hat{\varepsilon}$, i.e. $\omega = \Phi(\hat{\varepsilon})$. The damage eigenstrain is defined as $\varepsilon^d = \omega\varepsilon$. With the internal variable r, which records the largest equivalent strain in loading history, we define the closure of damage function as

$$C_{\hat{\varepsilon}} = \left\{ (\hat{\varepsilon}, r) \in R \times R \mid g(\hat{\varepsilon}, r) \le 0 \right\} \tag{6}$$

where $g(\hat{\varepsilon}, r) := \hat{\varepsilon} - r$. The damage evolution is defined as

$$\begin{aligned} \dot{\omega} &= \frac{1}{\vartheta} \left\langle g(\hat{\varepsilon}, r) \right\rangle \frac{\partial \Phi(\hat{\varepsilon})}{\partial \hat{\varepsilon}} \\ \dot{r} &= \frac{1}{\vartheta} \left\langle g(\hat{\varepsilon}, r) \right\rangle \end{aligned} \tag{7}$$

where $\langle \cdot \rangle$ is the Macaulay bracket and $\langle x \rangle = \frac{(x + |x|)}{2}$. The rate effect is controlled by ϑ. If $\vartheta \to 0$, the model becomes rate-independent, whereas if $\vartheta \to \infty$, the model coincides with the instantaneous elastic response. Various functions of damage parameter $\omega = \Phi(\hat{\varepsilon})$ have been proposed. Here, we adopt the simplest variant defined in Figure 4.

In Figure 4, S is the critical stress at the end of elastic process, G is the area under the stress/strain curve or the strain energy density. The damage parameter ω is defined as

$$\omega = \Phi(\hat{\varepsilon}) = \begin{cases} 0 & \hat{\varepsilon} < k_i \\ \frac{\omega_{max}(\hat{\varepsilon} - k_i)}{k_f - k_i} & k_i \le \hat{\varepsilon} \le k_f \\ \omega_{max} & \hat{\varepsilon} \ge k_f \end{cases} \tag{8}$$

$$k_i = \frac{S}{E_a} \quad k_f = \frac{-S + \sqrt{24GE_a - 3S^2}}{2E_a}, \tag{9}$$

where E_a is elastic modulus in the loading direction.

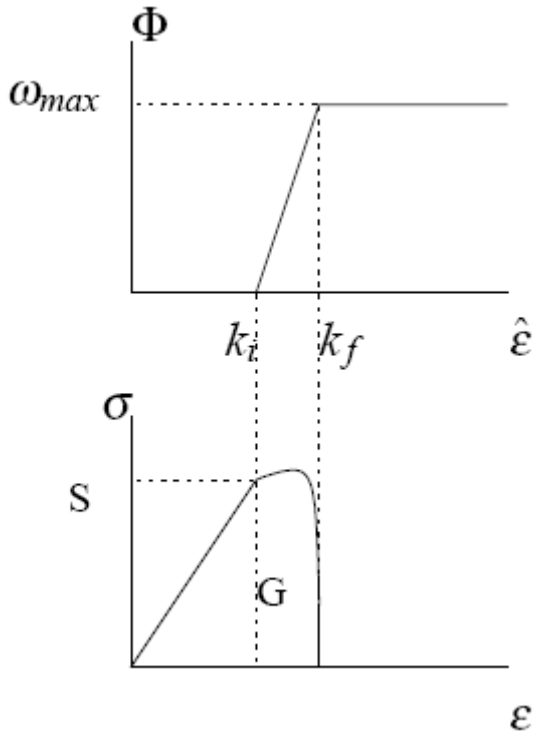

Figure 4. Relation between cumulative damage function Φ and stress/strain curve

3.2.2. The lock-in eigenstrain $\varepsilon^{c(mortar)}$

The lock-in eigenstrain ε^c is assumed to be a function $\varepsilon^c = \Psi(\tilde{\varepsilon})$ of the characteristic compressive strain defined as

$$\tilde{\varepsilon} = \sum_{I=1}^{3} \langle -\varepsilon_I \rangle, \tag{10}$$

where $\langle \cdot \rangle$ is the Macaulay bracket and ε_I is local principal strain. The function Ψ is characterized by three material parameters p_i, p_f and ε^c_{max} as (see also Figure 5)

$$\varepsilon^c = \Psi(\tilde{\varepsilon}) = \begin{cases} 0 & \tilde{\varepsilon} < p_i \\ \dfrac{\varepsilon^c_{max}(\tilde{\varepsilon} - p_i)}{p_f - p_i} & p_i \le \tilde{\varepsilon} \le p_f \\ \varepsilon^c_{max} & \tilde{\varepsilon} \ge p_f \end{cases} \tag{11}$$

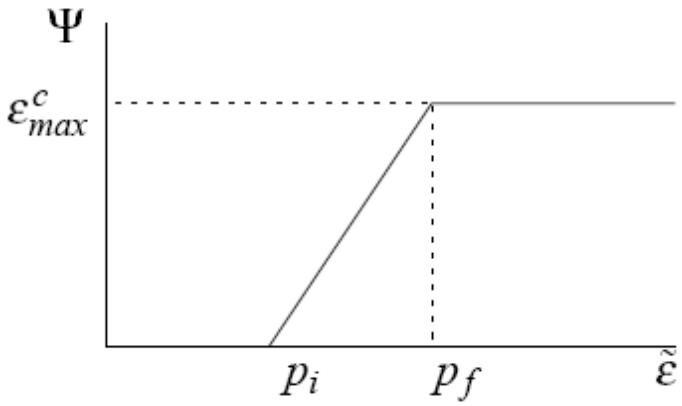

Figure 5. Relation between Ψ and characteristic strain $\tilde{\varepsilon}$

3.3. Numerical implementation

Recalling the internal variables a, b, and r, and defining the internal variable s to record the largest characteristic compressive strain $\tilde{\varepsilon}$ in the loading history, the algorithm in Box 1 describes an iterative scheme for updating multiple eigenstrains. The algorithm takes advantage of the reduced order equation (A10) given in the Appendix. Boxes 1.1-1.3 give the corresponding subroutines for updating different eigenstrains.

Box 1. Main Algorithm: Updating multiple eigenstrains in concrete (the reduced order unit cell problem)
Given microscopic variables (subscripts denoting the time step):

Microscopic strain $\varepsilon_n^{(mortar)}$, $\varepsilon_n^{(agg.)}$

Plastic eigenstrain $\varepsilon_n^{p(mortar)}$, $\varepsilon_n^{p(agg.)}$, and plastic internal variables

Damage eigenstrain $\varepsilon_n^{d(mortar)}$, and damage internal variables

Lock-in eigenstrain $\varepsilon_n^{c(mortar)}$, and lock-in internal variable

and macroscopic strain $\bar{\varepsilon}_n$, at time t_n, strain increment $\Delta\bar{\varepsilon}_{n+1}$ between t_n and t_{n+1}.

Find the above micro- and macroscopic variables at time t_{n+1}.

1. Let $\bar{\varepsilon}_{n+1} = \bar{\varepsilon}_n + \Delta\bar{\varepsilon}_{n+1}$, $\Delta t = t_{n+1} - t_n$.
2. Calculate the macroscale principal strain $\bar{\varepsilon}_{I_{n+1}}$.
3. Calculate the macroscale volumetric strain $\Xi_{n+1} = \sum_{I=1}^{3} \bar{\varepsilon}_{I_{n+1}}$.
4. Using $\varepsilon_n^{(mortar)}, \varepsilon_n^{(agg.)}$ as initial values, apply Newton Method to solve for $\varepsilon_{n+1}^{(mortar)}, \varepsilon_{n+1}^{(agg.)}$ from the equations (see equation (A9) in the Appendix)

$$\varepsilon_{ij_{(n+1)}}^{(mortar)} - P_{ijkl}^{(mortar.,mortar)}\left(\varepsilon_{kl_{(n+1)}}^{p(mortar)} + \varepsilon_{kl_{(n+1)}}^{d(mortar)} + \varepsilon_{kl_{(n+1)}}^{c(mortar)}\right) - P_{ijkl}^{(mortar.,agg.)}\varepsilon_{kl_{(n+1)}}^{p(agg.)} = A_{ijkl}^{(mortar)}\bar{\varepsilon}_{kl_{(n+1)}}$$

$$\varepsilon_{ij_{(n+1)}}^{(agg.)} - P_{ijkl}^{(agg.,agg.)}\varepsilon_{kl_{(n+1)}}^{p(agg.)} - P_{ijkl}^{(agg.,mortar)}\left(\varepsilon_{kl_{(n+1)}}^{p(mortar)} + \varepsilon_{kl_{(n+1)}}^{d(mortar)} + \varepsilon_{kl_{(n+1)}}^{c(mortar)}\right) = A_{ijkl}^{(agg.)}\bar{\varepsilon}_{kl_{(n+1)}}$$

For each iteration of the Newton Method:

(a) update the eigenstrains $\varepsilon_{n+1}^{p\ (mortar)}$ and $\varepsilon_{n+1}^{p\ (agg.)}$ using the subroutine in Box 1.1.

(b) update the eigenstrain $\varepsilon_{n+1}^{d\ (mortar)}$ using the subroutine in Box 1.2.

(c) update the eigenstrain $\varepsilon_{n+1}^{c\ (mortar)}$ using the subroutine in Box 1.3.

5. Let $(\cdot)_n = (\cdot)_{n+1}$.

Box 1.1. Subroutine for updating plastic eigenstrain ε_{n+1}^{p}

Given eigenstrain ε_n^p , plastic internal variables a_n , b_n , microscopic strain ε_{n+1} , and macroscopic volumetric strain Ξ_{n+1} .

Find ε_{n+1}^{p}, a_{n+1}, b_{n+1}.

If $\Xi_{n+1} > 0$, then (tensile loading):

$\varepsilon_{n+1}^{p} = \varepsilon_n^p$, $a_{n+1} = a_n$, $b_{n+1} = b_n$.

Else (compressive loading):

(a) find the deviator $e_{n+1} = \varepsilon_{n+1} - \frac{1}{3}(tr[\varepsilon_{n+1}])I$.

(b) compute the trial stress $\zeta_{n+1}^{trial} = 2\mu(e_{n+1} - e_n^p) - b_n$.

(c) check the yield condition $f_{n+1} := \| \zeta_{n+1}^{trial} \| - \sqrt{2/3}(\sigma_Y + \theta \overline{H} a_n)$. if $f_{n+1} > 0$, go to next step;

else $\Delta\gamma_{n+1} = 0$, go to step (f).

(d) calculate the consistency parameter $\Delta\gamma_{n+1} = \frac{f_{n+1}}{2\mu + \frac{2}{3}\overline{\overline{H}}}$.

(e) calculate the unit vector normal to von Mises yield surface $n_{n+1} = \frac{\zeta_{n+1}^{trial}}{\| \zeta_{n+1}^{trial} \|}$.

(f) update the plastic strain $\varepsilon_{n+1}^{p} = \varepsilon_n^p + \Delta\varepsilon_{n+1}^{p}$, where $\Delta\varepsilon_{n+1}^{p} = \Delta\gamma_{n+1} n_{n+1}$.

Box 1.2. Subroutine for updating damage eigenstrain ε^d_{n+1}

Given eigenstrain ε^d_n, damage internal variables ω_n, r_n, microscopic strain ε_{n+1}, time interval Δt and macroscopic volumetric strain Ξ_{n+1}.

Find ε^d_{n+1}, ω_{n+1}, r_{n+1}.

If $\Xi_{n+1} > 0$, then (tensile loading):

(a) find the local principal strain $\varepsilon_{I_{(n+1)}}$ by $\varepsilon_{ij_{(n+1)}}$.

(b) compute the equivalent strain $\hat{\varepsilon}_{n+1} = \sqrt{\sum_{I=1}^{3} [[\varepsilon_{I_{(n+1)}}]]^2}$, where $[[x]] = \begin{cases} x & x \geq 0 \\ cx & x < 0 \end{cases}$, c is material parameter indicating damage contribution from compression.

(c) if $\hat{\varepsilon}_{n+1} \leq r_n$ then $r_{n+1} = r_n$, $\omega_{n+1} = \omega_n$

else

$$r_{n+1} = \frac{r_n + \frac{\Delta t}{\vartheta}\hat{\varepsilon}_{n+1}}{1 + \frac{\Delta t}{\vartheta}}, \quad \omega_{n+1} = \omega_n + (r_{n+1} - r_n)\frac{\partial \Phi(\hat{\varepsilon}_{n+1})}{\partial \hat{\varepsilon}_{n+1}}$$

end if

(d) calculate the damage eigenstrain $\varepsilon^d_{n+1} = \omega_{n+1}\varepsilon_{n+1}$.

Else (compressive loading):

Box 1.3. Subroutine for updating eigenstrain ε^c_{n+1}

Given eigenstrain ε^c_n, lock-in internal variables s_n, microscopic strain ε_{n+1}, and macroscopic volumetric strain Ξ_{n+1}.

Find ε^c_{n+1}, s_{n+1}.

If $\Xi_{n+1} > 0$, then (tensile loading):

$s_{n+1} = s_n$, $\varepsilon^c_{n+1} = \varepsilon^c_n$.

Else (compressive loading):

(a) find the local principal strain $\varepsilon_{I_{(n+1)}}$ by $\varepsilon_{ij_{(n+1)}}$.

(b) compute the characteristic strain $\tilde{\varepsilon}_{n+1} = \sum_{I=1}^{3} \left\langle -\varepsilon_{I_{(n+1)}} \right\rangle$.

(c) if $\tilde{\varepsilon}_{n+1} \leq s_n$ then

$s_{n+1} = s_n$, $\varepsilon^c_{n+1} = \varepsilon^c_n$

else

$s_{n+1} = \tilde{\varepsilon}_{n+1}$, $\varepsilon^c_{n+1} = \Psi(\tilde{\varepsilon}_{n+1})$

4. Numerical Example: Penetration on Concrete Target

4.1. Unit cell of concrete

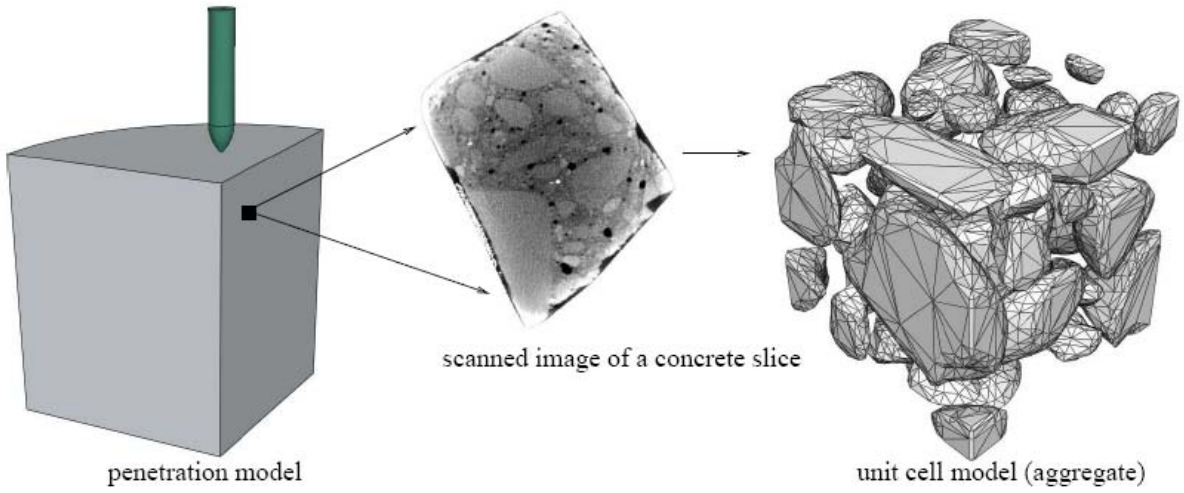

Figure 6. Construction of the unit cell model from digital image of concrete sample

We start with a construction of the unit cell model of concrete. The concrete type is given in Section 2. We assume that crushed limestone constitute the aggregate phase whereas the remaining material composes the mortar phase. The volume fraction of aggregate is 42% and the largest aggregate size is approximately 10mm. The geometry of the unit cell is reconstructed from scanned images in various cross-sections of the concrete sample. The finite element mesh is then generated from the grey-level digital images [30]. Figure 6 shows the unit cell model used in the present study. A thin mortar phase is formed to encompass the unit cell so that periodic boundary conditions could be imposed on the mortar phase only as shown in Figure 7.

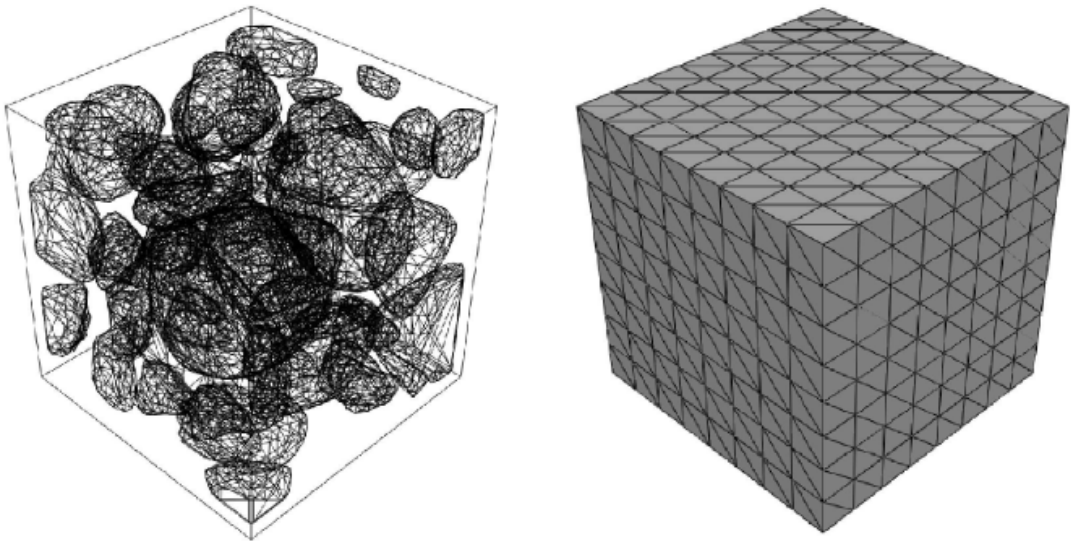

Figure 7. Finite element mesh of unit cell model for concrete

4.2. Prediction of projectile penetration

The numerical model was implemented in ABAQUS [31]. The constitutive law of concrete was coded using Fortran subroutines in UMAT/VUMAT of ABAQUS. Material parameters were calibrated using laboratory tests [8]. We adopted the test data set of concrete from [32] for the purpose of comparison. The length and diameter of the specimens were on average 111.37mm and 50.4mm, respectively. We used unconfined compression and uniaxial compression tests to calibrate material parameters for each phase. The responses for the two tests are shown in Figure 8 and Figure 9. The calibrated microscopic material parameters are listed as in Table 3.

Table 3. Calibrated microscopic material parameters of concrete

Phase	E (MPa)	ν	σ_Y (MPa)	$\overline{H}$ (MPa)	θ		
Mortar	40000.0	0.2	11.0	2000	1		
Aggregate	60000.0	0.2	75.0	4000	1		
Phase	S (MPa)	G (MJ/m^3)	c	p_i	p_f	ε_{max}^c	ϑ
Mortar	1.0	1.25×10^{-5}	0.0	0.0025	0.145	0.052	0.05

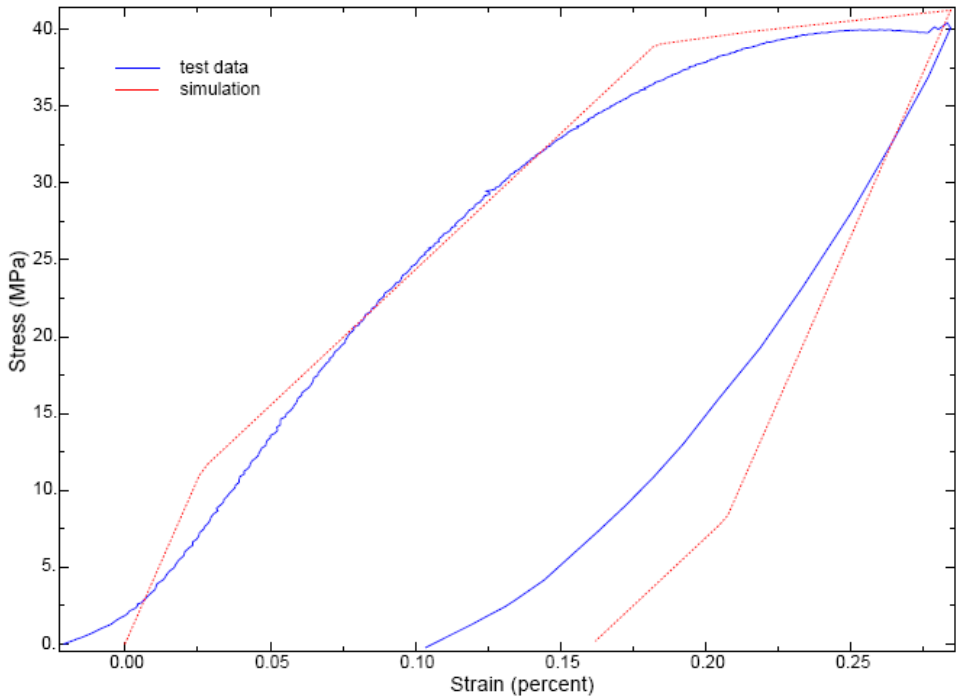

Figure 8. The response comparison in unconfined compression

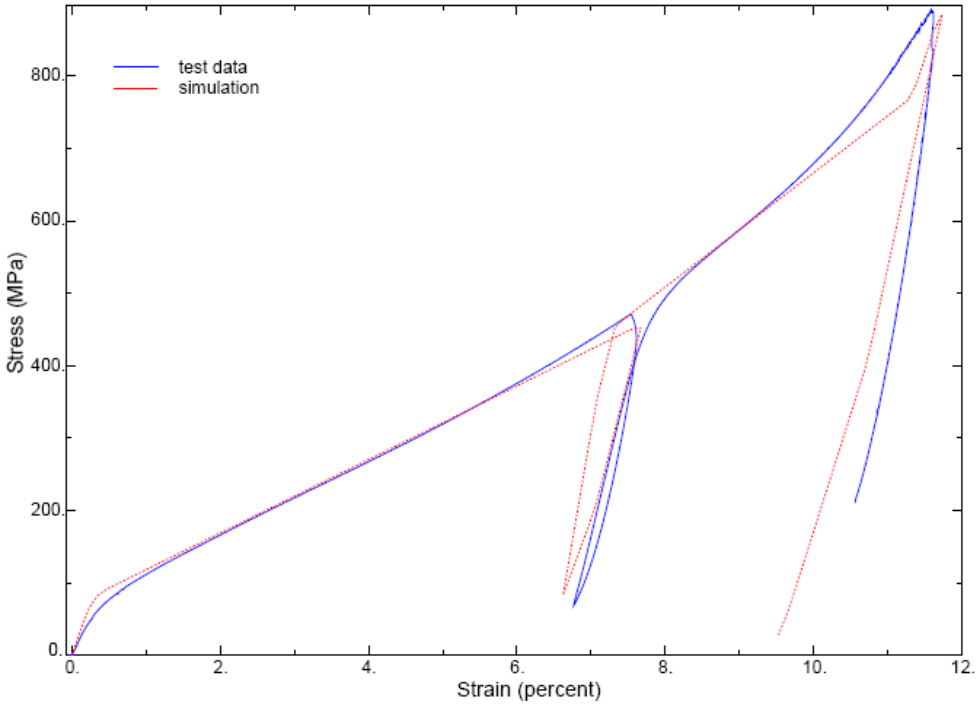

Figure 9. The response comparison of uniaxial compression

With material parameters for each phase defined, we constructed the finite element model for concrete target and projectile. The finite element size in the penetrating region was 10mm. The projectile was fired at five different velocities, which are $238.1m/s$, $275.7m/s$, $314m/s$, $369.5m/s$, and $456.4m/s$. Two types of properties were investigated, penetration depth and projectile deceleration [32]. The depth comparison between the test data and simulation are listed in Table 4. Figures 10-14 show the deceleration comparison for different striking velocities V_s.

Table 4. Penetration depth comparison for 1.83m diameter concrete targets

Striking Velocity (m/s)	Penetration Depth (m)	Simulated Depth (m)
238.1	0.30	0.284
275.7	0.38	0.365
314.0	0.45	0.457
369.5	0.53	0.60
456.4	0.94	0.89

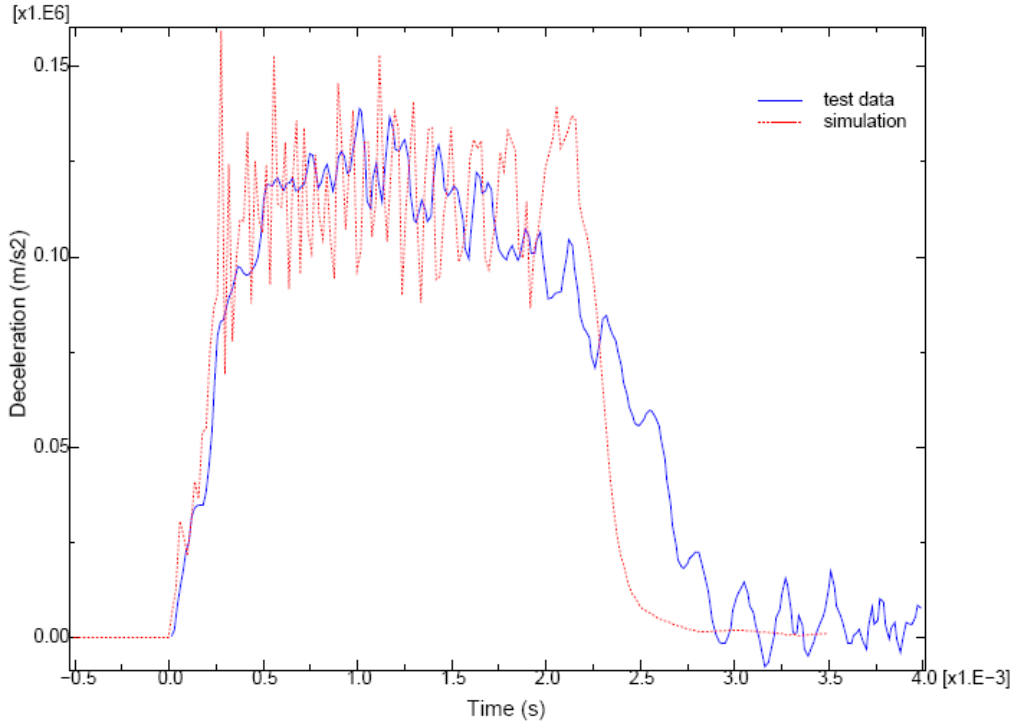

Figure 10. Projectile deceleration comparison under $V_s = 238.1 m/s$

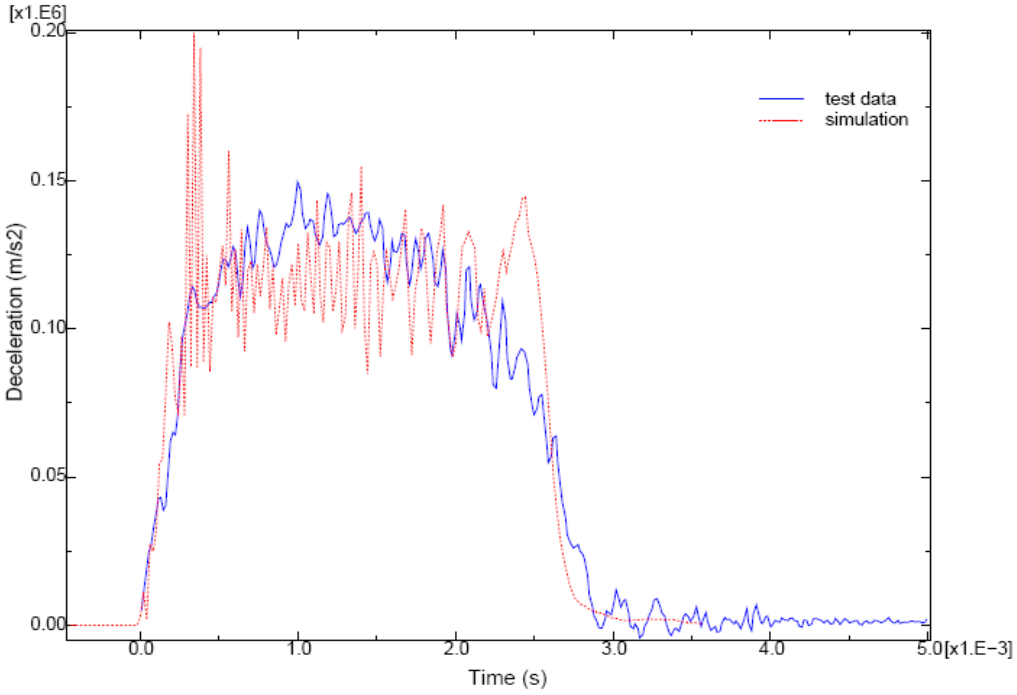

Figure 11. Projectile deceleration comparison under $V_s = 275.7 m/s$

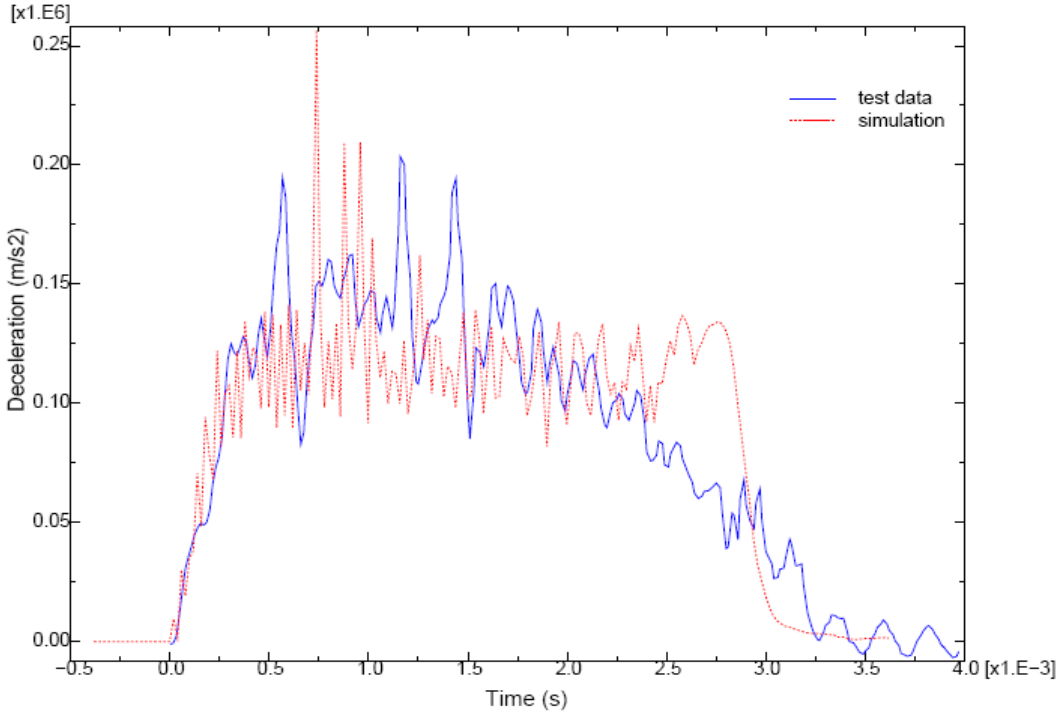

Figure 12. Projectile deceleration comparison under $V_s = 314 m/s$

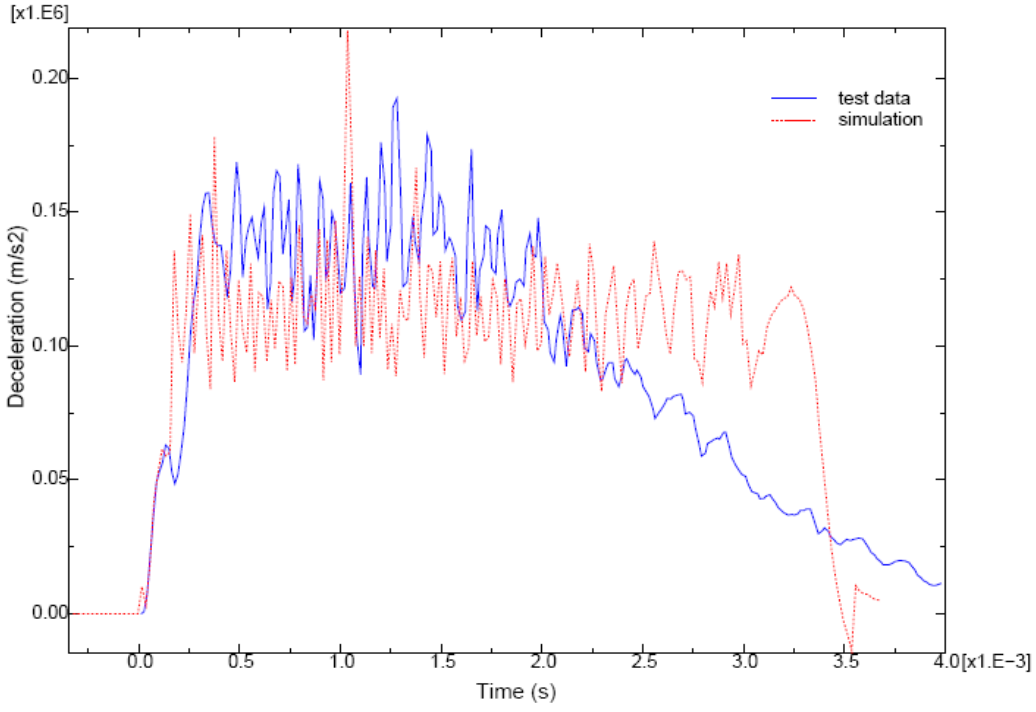

Figure 13. Projectile deceleration comparison under $V_s = 369.5 m/s$

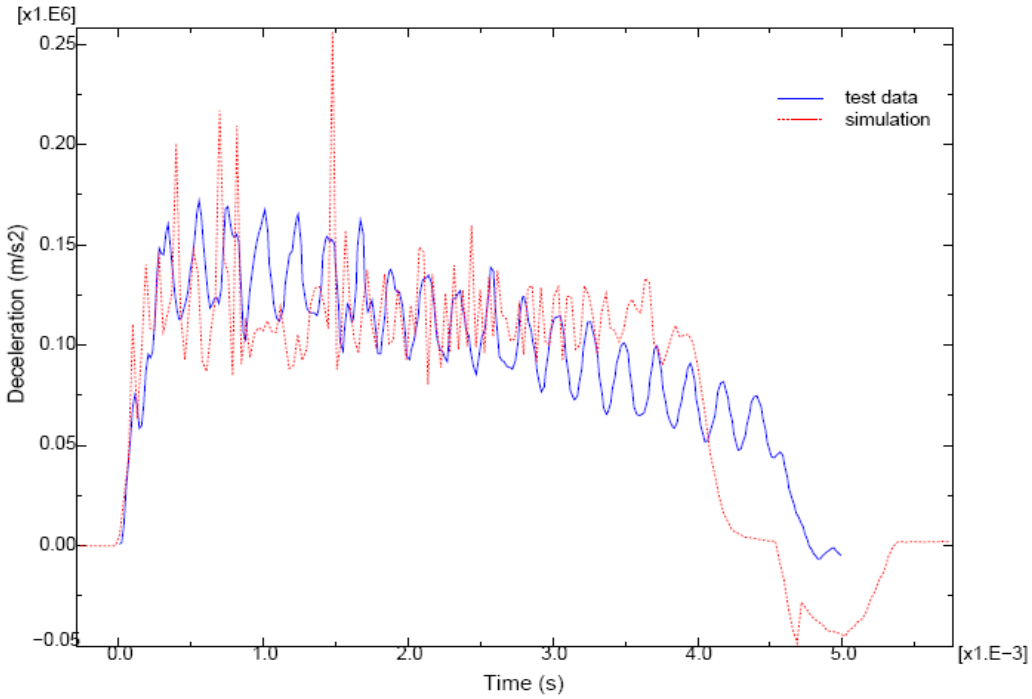

Figure 14. Projectile deceleration comparison under $V_s = 456.4 m/s$

The depth and deceleration prediction agreed reasonably well with the test data. In this study, we also investigated the damage parameter in the mortar phase of the concrete target at various projectile velocities as shown in Figure 15. It can be seen that the damage level increases with increase in striking velocity. The damage contours depicted in Figure 15 provide the qualitative shape of the crater during the penetration.

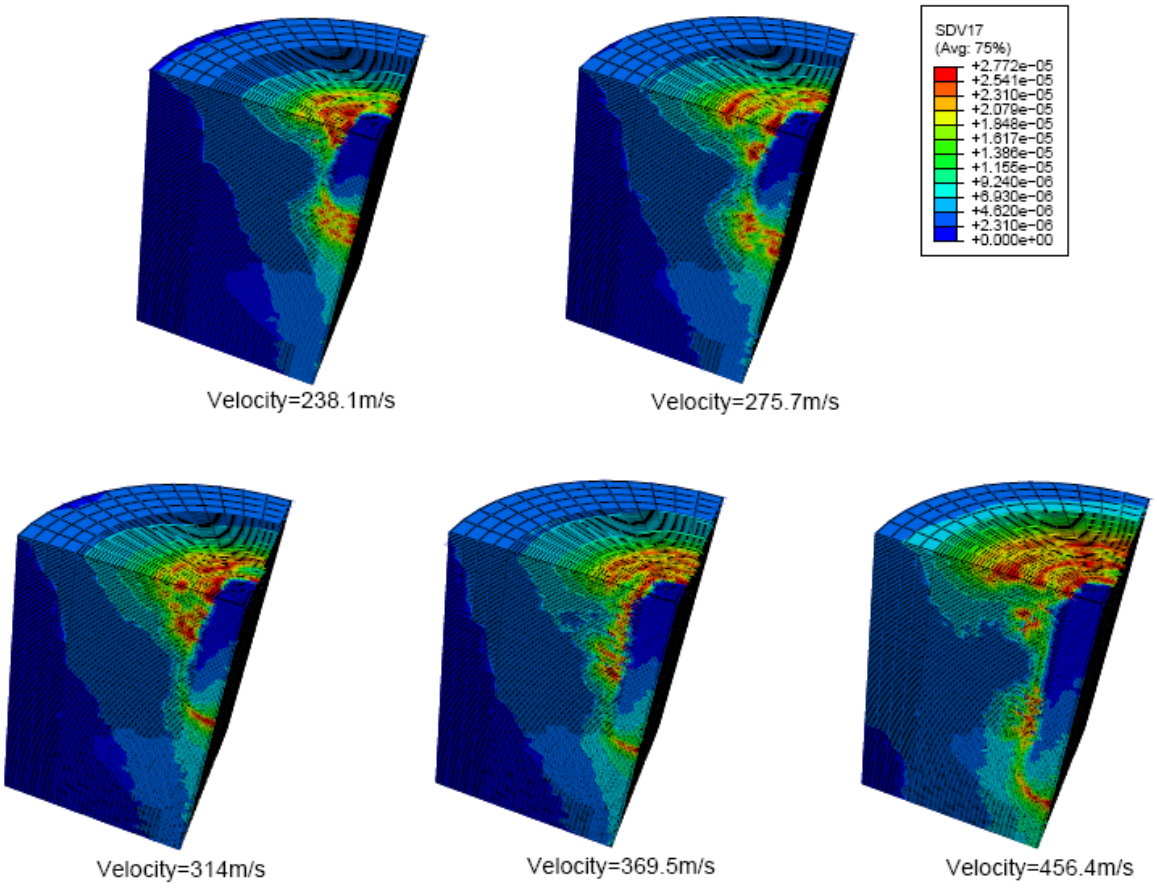

Figure 15. Equivalent damage strain in the mortar phase of concrete target penetrated by projectiles at various striking velocities

5. Conclusions and future research directions

A multiscale approach for predicting penetration of projectiles into concrete targets has been explored as an alternative to conventional methods based on either empirical-analytical approaches, experimental techniques or numerical approaches employing phenomenological or rules-of-mixture constitutive models of concrete. The multiscale approach presented in this paper is based on eigendeformation-based homogenization which approximates the solution fields in the unit cell in terms of the residual-free functions and consequently avoids costly equilibrium calculations. The inelastic behavior of concrete is modeled using pore compaction (or lock-in) and rate-dependent damage eigenstrains in the mortar phase as well as plastic eigenstrains in both the aggregates and mortar. The method has been validated on a rigid projectile penetration problem for which experimental data exists.

Future studies will focus on the following three issues: (i) consideration of steel

reinforcement, (ii) accounting for uncertainty in the concrete microstructure, (iii) development of the mechanistic approach to pore compaction which so far has been accounted for phenomenologically. To account for steel reinforcement we will employ a three-scale reduced homogenization approach [23,24,26] where the concrete microstructure will be considered at the microscale and a rebar embedded in a homogenized concrete will comprise the mesoscale. To account for the uncertainty in the concrete microstructure we will employ a combination of the reduced-order and stochastic homogenization methods. To account for pore compaction, development of large deformation eigendeformation based homogenization will be pursued.

6. Acknowledgment

The authors wish to thank Dr. Brian Plunkett and Dr. Martin Schmidt from the Computational Mechanics Branch at USAF Research Laboratory for their guidance and financial support.

Appendix A. Brief Theory of Reduced-Order Homogenization

A.1. Mathematical homogenization

In the mathematical homogenization theory, various fields are assumed to be a function of the macroscopic coordinates, x, and as the microscopic coordinate system, $y = x/\zeta$, where ζ is a small positive parameter. Combining the governing equations (1-3) with the asymptotic expansions

$$\begin{aligned} u_i(x,y,t) &= u_i^0(x,t) + \zeta u_i^1(x,y,t) + \cdots \\ \varepsilon_{ij}(x,y,t) &= \varepsilon_{ij}^0(x,y,t) + \zeta \varepsilon_{ij}^1(x,y,t) + \cdots \\ \sigma_{ij}(x,y,t) &= \sigma_{ij}^0(x,y,t) + \zeta \sigma_{ij}^1(x,y,t) + \cdots \\ {}^I\mu_{ij}(x,y,t) &= {}^I\mu_{ij}^0(x,y,t) + \zeta {}^I\mu_{ij}^1(x,y,t) + \cdots \end{aligned} \tag{A1}$$

yields the unit cell problem

$$\left\{ L_{ijkl}(y) \left[\bar{\varepsilon}_{kl}(x,t) + u_{k,y_l}^1(x,y,t) - \sum_I {}^I\mu_{kl}^0(x,y,t) \right] \right\}_{,y_j} = 0 \tag{A2}$$

from which the macroscale stress can be computed

$$\bar{\sigma}_{ij,j}(x,t) = \frac{1}{\Theta} \int_\Theta L_{ijkl}(y) \left(\bar{\varepsilon}_{kl}(x,t) + u_{k,y_l}^1(x,y,t) - \sum_I {}^I\mu_{kl}^0(x,y,t) \right) dy \tag{A3}$$

where Θ is the unit cell domain, while $\bar{\sigma}_{ij}$ and $\bar{\varepsilon}_{ij}$ are macroscale stress and strain, respectively.

A.2. Reduced order multiscale system

Following [23], the microscale displacement field $u_i^1(x,y,t)$ is constructed so that the stress field in the unit cell would automatically satisfy equilibrium equations. This is accomplished by introducing eigenstrain ${}^I\mu_{ij}^0$ and eigenseparations $\delta_{\hat{n}}$

$$\begin{aligned} u_i^1(x,y,t) &= u_i^{el}(x,y,t) + \sum_I {}^I u_i^{eig\_stra}(x,y,t) + u_i^{eig\_disp}(x,y,t) \\ &= H_{ikl}\bar{\varepsilon}_{kl}(x,t) + \sum_I \int_\Theta {}^I h_{ikl}^{stra}(y,\hat{y})\,{}^I\mu_{kl}^0(x,\hat{y},t)d\hat{y} \\ &+ \int_S h_{i\hat{n}}^{disp}(y,\hat{y})\delta_{\hat{n}}(x,\hat{y},t)d\hat{y} \end{aligned} \tag{A4}$$

The resulting microscale displacement gradients are given by

$$\begin{aligned} u_{i,y_j}^1(x,y,t) &= G_{ijkl}\bar{\varepsilon}_{kl}(x,t) + \sum_I \int_\Theta {}^I g_{ijkl}^{stra}(y,\hat{y})\,{}^I\mu_{kl}^0(x,\hat{y},t)d\hat{y} \\ &+ \int_S g_{ij\hat{n}}^{disp}(y,\hat{y})\delta_{\hat{n}}(x,\hat{y},t)d\hat{y} \end{aligned} \tag{A5}$$

where G_{ijkl}, ${}^I g_{ijkl}^{stra}$, and $g_{ij\hat{n}}^{disp}$ are influence functions for macroscale strain, eigenstrain, and eigendisplacement, respectively, which can be computed by solving a sequence of elastic boundary value problems prior to nonlinear macro analysis. A reduced order model is obtained by discretizing eigenstrain and eigenseparation fields as

$$\begin{aligned} {}^I\mu_{ij}^0(x,y,t) &= \sum_{\alpha=1}^{n_I} {}^I N^{(\alpha)}(y)\,{}^I\bar{\mu}_{ij}{}^{(\alpha)}(x,t) \\ \delta_{\hat{n}}(x,\tilde{y},t) &= \sum_{\xi=1}^{m} N^{(\xi)}(\tilde{y})\bar{\delta}_{\hat{n}}^{(\xi)}(x,t) \end{aligned} \tag{A6}$$

where n_I and m are the numbers of partitions of phases and interfaces respectively, ${}^I\bar{\mu}_{ij}{}^{(\alpha)}$ and $\bar{\delta}_{\hat{n}}^{(\xi)}$ are the average eigenstrain and eigendisplacement in the phase partition α and interface partition ξ, respectively. $N^{(\alpha)}(y)$ is a piecewise constant shape function defined as

$$N^{(\alpha)}(y) = \begin{cases} 1 & y \in \Theta^{(\alpha)}, \\ 0 & y \in \Theta^{(\alpha)}. \end{cases} \tag{A7}$$

$N^{(\xi)}(\tilde{\mathbf{y}})$ is a linear combination of piecewise linear finite element shape functions defined over partition ξ.

Combining the unit cell equations (A2) with the decomposition (A5) with the above discretization yields the reduced system of equations:

Reduced-Order Microscale Unit Cell Problem:

$$\begin{aligned}&\varepsilon_{ij}^{(\beta)}(x,t)-\sum_{I=1}^{N}\sum_{\alpha=1}^{n_I}{}^{I}P_{ijkl}^{(\beta\alpha)I}\bar{\mu}_{kl}^{(\alpha)}(x,t)-\sum_{\xi=1}^{m}Q_{ij\hat{n}}^{(\beta\xi)}\bar{\delta}_{\hat{n}}^{(\xi)}(x,t)=A_{ijkl}^{(\beta)}\bar{\varepsilon}_{kl}(x,t)\\&-\sum_{I=1}^{N}\sum_{\alpha=1}^{n_I}{}^{I}C_{\hat{n}kl}^{(\eta\alpha)I}\bar{\mu}_{kl}^{(\alpha)}(x,t)+t_{\hat{n}}^{(\eta)}(x,t)-\sum_{\xi=1}^{m}D_{\hat{n}\hat{m}}^{(\eta\xi)}\bar{\delta}_{\hat{m}}^{(\xi)}(x,t)=B_{\hat{n}kl}^{(\eta)}\bar{\varepsilon}_{kl}(x,t)\end{aligned}\tag{A9}$$

Reduced-Order Macroscale Stress Updating:

$$\bar{\sigma}_{ij}(x,t)=\bar{L}_{ijkl}\bar{\varepsilon}_{kl}(x,t)+\sum_{I=1}^{N}\sum_{\alpha=1}^{n_I}{}^{I}\bar{E}_{ijkl}^{(\alpha)I}\bar{\mu}_{kl}^{(\alpha)}(x,t)+\sum_{\xi=1}^{m}\bar{F}_{ij\hat{n}}^{(\xi)}\bar{\delta}_{\hat{n}}^{(\xi)}(x,t)\tag{A10}$$

where $t_{\hat{n}}=G(\bar{\delta}_{\hat{n}})$ represents the traction along interface. All coefficient tensors in the reduced-order system, such as ${}^{I}P_{ijkl}$, $Q_{ij\hat{n}}$, A_{ijkl}, ${}^{I}C_{\hat{n}ij}$, $D_{\hat{n}\hat{m}}$, $B_{\hat{n}ij}$, $\bar{L}_{ijkl}$, ${}^{I}\bar{E}_{ijkl}$, and $\bar{F}_{ij\hat{n}}$, are determined prior to the nonlinear analysis in the preprocessing stage. The detailed formulation can be found in [23,24].

References

[1] C.Y.Tham. Numerical and empirical approach in predicting the penetration of a concrete target by an ogive-nosed projectile. *Finite Elements in Analysis and Design*, 42:1258–1268, 2006.

[2] M.J.Forrestal and D.Y.Tzou. A spherical cavity-expansion penetration model for concrete targets. *Int. Journal of Solids and Structures*, 34:4127–4146, 1997.

[3] D.J.Frew, S.J.Hanchak, M.L.Green, and M.J.Forrestal. Penetration of concrete targets with ogive-nose steel rods. *Int. Journal of Impact Engineering*, 21:489–497, 1998.

[4] M.J.Forrestal, D.J.Frew, J.P.Hickerson, and T.A.Rohwer. Penetration of concrete targets with deceleration-time measurements. *Int. Journal of Impact Engineering*, 28:479–497, 2003.

[5] M.J.Forrestal, D.J.Frew, S.J.Hanchak, and N.S.Brar. Penetration of grout and concrete targets with ogive-nose steel projectiles. *Int. Journal of Impact Engineering*, 18:465–476, 1996.

[6] M.Ortiz and E.P.Popov. Plain concrete as a composite material. *Mechanics of Materials*, 1:139–150, 1982.

[7] C.D.Foster, R.A.Regueiro, A.F.Fossum, and R.I.Borja. Implicit numerical integration of a three-invariant, isotropic/kinematic hardening cap plasticity model for geomaterials. *Computer Methods in Applied Mechanics and Engineering*, 194:5109–5138, 2005.

[8] T.L.Warren, A.F.Fossum, and D.J.Frew. Penetration into low-strength (23MPa) concrete:

Target characterization and simulations. *Int. Journal of Impact Engineering*, 30:477–503, 2004.
[9] M.Polanco-Loria, O.S.Hopperstad, T.Borvik, and T.Berstad. Numerical predictions of ballistic limits for concrete slabs using a modified version of the HJC concrete model. *Int. Journal of Impact Engineering*, 35:290–303, 2008.
[10] M.R.Salari, S.Saeb, K.J.Willam, S.J.Patchet, and R.C.Carrasco. A coupled elastoplastic damage model for geomaterials. *Computer Methods in Applied Mechanics and Engineering*, 193:2625–2643, 2004.
[11] J.Y.Wu, J.Li, and R.Faria. A energy release rate-based plastic-damage model for concrete. *Int. Journal of Solids and Structures*, 43:583–612, 2006.
[12] M.Ortiz. A constitutive theory for the inelastic behavior of concrete. *Mechanics of Materials*, 4:67–93, 1985.
[13] M.Ortiz. An analytical study of the localized failure modes of concrete. *Mechanics of Materials*, 6:159–174, 1987.
[14] D.Tikhomirov and E.Stein. Finite element computations of anisotropic continuum damage in reinforced concrete. *Computers and Structures*, 79:2249–2260, 2001.
[15] J.Lubliner, J.Oliver, S.Oller, and E.Onate. A plastic-damage model for concrete, *International Journal of Solids and Structures*, 25:299-326, 1989.
[16] J.W.Ju, P.J.M.Monteiro, and A.I.Rashed. On continuum damage of cement paste and mortar as affected by porosity and sand concentration, *J. of Eng. Mech., ASCE*, Vol. 115, No. 1, 105-130, Jan. 1989.
[17] Z.P.Bažant, F.C.Caner, I.Carol, M.D.Adley, and S.A.Akers. Microplane model M4 for concrete: I. Formulation with work-conjugate deviatoric stress. *J. of Eng. Mech. ASCE*, 126, 944-953. 2000a.
[18] G.Mounajed, F.Grondin, H.Dumontet, and A.Ben Hamid. Digital concrete: A multi-scale approach for the concrete behavior, *Journal of Computational Methods in Science and Engineering*, Volume 6, Number 5-6, 1472-7978, 2006.
[19] M.Hain and P.Wriggers. Computational homogenization of micro-structural damage due to frost in hardened cement paste, *Finite Elements in Analysis and Design*, Volume 44, Issue5 233-244, 2008.
[20] R.Lackner, H.A.Mang, and C.Pichler. Chapter 15. Computational Concrete Mechanics, in *Encyclopedia of Computational Mechanics*, *Part 2. Solids and Structures*, eds. E.Stein, R.de Borst, T.J.R.Hughes (eds.), 2004 John Wiley & Sons.
[21] G.Cusatis, D.Pelessone, A.Mencarelli, and J.T.Baylot. Simulation of reinforced concrete structures under blast and penetration through lattice discrete particle modeling. *Electronic Proceedings (CD) of IMECE 2007 - ASME International Mechanical Engineering Conferences & Exposition*, November 11-15, 2007, Seattle, USA.
[22] E.Schlangen. Experimental and numerical analysis of fracture processes in concrete. *Ph. D. Thesis*, Delft University of Technology, Delft, The Netherlands, 1993.
[23] J.Fish and Z.Yuan. N-scale model reduction theory, in *Bridging the Scales in Science and Engineering*, J. Fish (ed), Oxford University Press, 2008.
[24] Z.Yuan and J.Fish. Multiple scale eigendeformation-based reduced order homogenization. to appear in *Computer Methods in Applied Mechanics and Engineering*, 2008.
[25] C.Oskay and J.Fish. Eigendeformation-based reduced order homogenization. *Computer Methods in Applied Mechanics and Engineering*, 196:1216–1243, 2007.
[26] Z.Yuan and J.Fish. Hierarchical model reduction at multiple scales, to appear in

International Journal for Numerical Methods in Engineering, 2008.
[27] E.Gal and J.Fish. Anisotropic micromechanical creep damage model for composite materials: a reduced-order approach, *International Journal of Multiscale Computational Engineering*, Vol. 6, Issue 2, 113-121, 2008.
[28] E.Gal, Z.Yuan, W.Wu and J.Fish. A multiscale design system for fatigue life prediction, *International Journal of Multiscale Computational Engineering*, Vol. 5, Issue 6, 435-446, 2007.
[29] J.C.Simo and T.J.R.Hughes. *Computational Inelasticity*. Springer, 1998.
[30] G.Nagai and T.Yamada. Three-dimensional finite element modeling for concrete materials using digital image and embedded discontinuous element. *Int. Journal for Multiscale Computational Engineering*, 4:461–474, 2006.
[31] ABAQUS Product, http://www.simulia.com/
[32] D.J.Frew. Conventional strength portland cement (CSPC) concrete instrumented penetration results. *Technical report, Sandia National Laboratories*, 2001.

DISTRIBUTION LIST
AFRL-RW-EG-TR-2009-7066

DEFENSE TECHNICAL INFORMATION CENTER - 1 Electronic Copy (1 File & 1 Format)
ATTN: DTIC-OCA (ACQUISITION)
8725 JOHN J. KINGMAN ROAD, SUITE 0944
FT. BELVOIR VA 22060-6218

AFRL/RWOC-1 (STINFO Office) - 1 Hard (Color) Copy
AFRL/RW CA-N - STINFO Officer Provides Notice of Publication
AFRL/RWA - 1
AFRL/RWAC - 1